Carbon ionization from a quantum average-atom model up to gigabar pressures

Gérald Faussurier* and Christophe Blancard
CEA, DAM, DIF, F-91297 Arpajon, France and Université Paris-Saclay, CEA, LMCE, F-91680 Bruyères-le-Châtel, France

Mandy Bethkenhagen
École Normale Supérieure de Lyon, Université Lyon 1, Laboratoire de Géologie de Lyon, CNRS UMR 5276, F-69364 Lyon Cedex 07, France and University of Rostock, 18051 Rostock, Germany

(Received 18 March 2021; revised 28 July 2021; accepted 28 July 2021; published 25 August 2021)

We use a nonrelativistic average-atom model to calculate carbon ionization at megabar and gigabar pressures. The pressure is calculated using the stress-tensor method. The electronic electrical conductivity is also considered using the Kubo-Greenwood approach. Comparisons are made with quantum molecular dynamic simulations. A good agreement is obtained for the pressure between the average-atom model and the quantum molecular dynamic simulations in the regime of gigabar pressures. However, the discrepancy already seen with the PURGATORIO code for the average ionization deduced from the quantum molecular dynamic simulations is also observed here with the present average-atom model. Excellent agreement with the PURGATORIO code is found for the average ionization.

DOI: 10.1103/PhysRevE.104.025209

I. INTRODUCTION

The calculation of average ionization in dense plasmas is a long-standing problem [1]. This quantity can play a key role in the calculation of the equation of state, electrical conductivity, or absorption coefficients in warm and hot dense matter. There is no accepted definition of the average ionization. One reasonable solution is to use the electronic density at the boundary of the Wigner-Seitz cell [2]. In this way we obtain a quantity that is a smooth function with pressure ionization. It has been shown that it gives good results for the electrical resistivity calculated with the Ziman-Evans formula [3–6] when compared with experiment [7].

Recently, it has been proposed to extract the average ionization using quantum molecular dynamic (QMD) simulations [8]. The idea is to calculate the electronic electrical conductivity $\sigma(\omega)$ using the Kubo-Greenwood approach [9–11] where ω is the angular frequency, and to use a well-known sum rule obeyed by $\sigma(\omega)$ to derive an effective average ionization. Calculations have been done in carbon plasmas at gigabar pressures. Comparisons [8] with the PURGATORIO average-atom model [12,13] have shown that the QMD results are systematically about 0.5 higher than the average ionization predicted by the PURGATORIO code.

In this article, we propose to use a nonrelativistic quantum average-atom model (QAAM) to calculate the average ionization and the pressure to confirm or infirm the comparisons performed between the QMD simulations and the PURGATORIO code [8]. We consider carbon plasmas in local thermodynamic equilibrium (LTE) at megabar and gigabar pressures. The electronic electrical conductivity is also calculated using the Kubo-Greenwood method applied to the average-atom model [14–16]. The present work is organized as follows. We first present the 1D spherically symmetric QAAM model. The bound and free formulas for the electronic pressure are given [17] as well as the free-free electronic electrical conductivity expression based on the Kubo-Greenwood method. Second, we describe how the QMD simulations were done and how the pressure is calculated in this approach. The same methods are used in QAAM and the QMD simulations to compute the electronic and ionic parts of the pressure. The only difference is the treatment of the 3D effects in the QMD simulations. Numerical results are then presented. Comparisons between the QAAM results and the QMD and PURGATORIO code for the average ionization are performed. Comparisons are made for pressure and electrical conductivity between QAAM and QMD simulations. Finally, we present our conclusion in the last section.

II. THEORY

A. The quantum average-atom model QAAM

The nonrelativistic quantum average-atom model in the muffin-tin approximation to describe the electronic structure in dense plasmas is well known [12–14,18,19]. We assume that the electrons are in LTE at T_e and the ions at T_i. The electronic structure does not depend on T_i; only the equation of state depends on T_i. In this work, we suppose that $T_e = T_i = T$. We use the finite-temperature density-functional-theory (DFT) in the local density approximation (LDA) [20–22] to derive the average-atom equations. They read

$$\left[-\frac{\hbar^2}{2m_e}\nabla^2 - \frac{Z^2e^2}{r} + e^2\int d\mathbf{r}'\frac{n(r')}{|\,\mathbf{r}-\mathbf{r}'\,|} + V_{xc}(r)\right]\psi_a(\mathbf{r}) = \varepsilon_a\psi_a(\mathbf{r}), \quad (1)$$

where $\hbar$ is the reduced Planck constant, e the elementary charge, m_e the electron rest mass, and Z the nuclear charge. ε_a

*gerald.faussurier@cea.fr

is the one-electron energy. $a = (n, \ell)$ for bound states and $a = (\varepsilon, \ell)$ for continuum states. In this case, the one-electron energy is simply $\varepsilon = \hbar^2 k^2/2m_e$. $V_{xc}(r)$ is the finite-temperature exchange-correlation potential [23]. We are using a fit of a finite-temperature exchange-correlation functional in the LDA framework. This fit has been obtained from the equation of state of the finite-temperature electron liquid derived using the Singwi-Tosi-Land-Sjölander approximation. Moreover, it is difficult to know how the present finite-temperature exchange-correlation potential compared with, for instance, the finite-temperature exchange potential of Gupta and Rajagopal [24]. The wave function $\psi_a(\mathbf{r})$ is equal to

$$\psi_a(\mathbf{r}) = \frac{1}{r} P_a(r) Y_{\ell_a}^{m_a}(\theta, \phi) \chi_{\sigma_a}, \tag{2}$$

where $Y_\ell^m(\theta, \phi)$ is a spherical harmonic and χ_σ is a two-component electron spinor. The bound and free radial wave functions are normalized such that

$$\int_0^{+\infty} dr P_{n\ell}(r) P_{n'\ell}(r) = \delta_{nn'} \tag{3}$$

and

$$\int_0^{+\infty} dr P_{\varepsilon\ell}(r) P_{\varepsilon'\ell}(r) = \delta(\varepsilon - \varepsilon'). \tag{4}$$

The total electron density of the average atom is $n(r) = n_b(r) + n_f(r)$ where

$$4\pi r^2 n_b(r) = \sum_{n\ell} \frac{2(2\ell+1)}{1 + e^{(\varepsilon_{n\ell} - \mu)/k_B T}} P_{n\ell}(r)^2 \tag{5}$$

and

$$4\pi r^2 n_f(r) = \sum_{\ell} \int_0^{+\infty} d\varepsilon \frac{2(2\ell+1)}{1 + e^{(\varepsilon - \mu)/k_B T}} P_{\varepsilon\ell}(r)^2. \tag{6}$$

k_B is the Boltzmann constant. The chemical potential μ is determined such that

$$\int_0^{R_{WS}} 4\pi r^2 n(r)\, dr = Z. \tag{7}$$

R_{WS} is the Wigner-Seitz radius with $4\pi R_{WS}^3 N_i/3 = 1$ where N_i is the ion density. The Wigner-Seitz cell is neutral. For $r > R_{WS}$, $V_{ei}(r) = 0$ where

$$V_{ei}(r) = -\frac{Z^2 e^2}{r} + e^2 \int d\mathbf{r}' \frac{n(r')}{|\,\mathbf{r} - \mathbf{r}'\,|} + V_{xc}(r). \tag{8}$$

The Kohn-Sham potential $V_{ei}(r)$ is short-range. These equations are solved self-consistently using the RADIAL package [25]. The maximum orbital quantum-number $\ell_>$ for the continuum states is set equal to 15. We are using the trick proposed by Blenski and Ishikawa [18] to take into account high values of the orbital quantum-number for the continuum states using a well-known sum rule obeyed by the Bessel functions. We have checked that the summation converged rapidly with $\ell_>$ so that $\ell_> = 15$ is a very good choice in the calculations presented in this work. We do not describe the density of states between -0.005 Ry and 0.0001 Ry. An initial guess of $V_{ei}(r)$ is done using a Thomas-Fermi-Dirac-Amaldi potential [26] to start the self-consistent process. The bound and free radial wave functions are then calculated within this initial potential and the self-consistent process is launched. In this work, we have used a two-step relaxation process on $V_{ei}(r)$. We can do better by relaxing directly the total radial density $n(r)$ before calculating $V_{ei}(r)$, which is far more efficient. In practice, for the first three steps, we relax $V_{ei}(r)$ and then $n(r)$. Note that the calculations using the RADIAL package may take some time. By this, we mean that in this work it can take 15 to 20 min for the process to achieve convergence for one point in temperature and mass density on a usual workstation. We can achieve convergence in a few minutes using the routine FREEWA from the University College London distorted-wave code [26] to compute the free wave functions. However, this routine is sometimes less accurate to obtain the phase shifts than the routine SFREE of the RADIAL package. Note that there is a deep problem concerning the charge conservation in the average-atom model using the muffin-thin approximation that cannot simply be solved using simple ionic reference-systems such as hard-sphere, one-component plasma, or soft-sphere systems [27]. In order to calculate the electronic pressure, we use the stress-tensor approach [17]. The neutrality is ensured only inside the Wigner-Seitz cell. For the free part, we have

$$P_{\text{contin}} = \frac{\hbar^2}{24\pi m_e} \int_0^{+\infty} d\varepsilon f(\varepsilon) \sum_\ell 2(2\ell+1) \left\{ \left[\frac{d}{dr} \left(\frac{P_{\varepsilon\ell}(r)}{r} \right) \right]^2 + k^2 \left(\frac{P_{\varepsilon\ell}(r)}{r} \right)^2 + \frac{\ell(\ell+1)}{r^2} \left(\frac{P_{\varepsilon\ell}(r)}{r} \right)^2 \right\}_{R_{WS}}. \tag{9}$$

This expression is consistent with the one derived by Johnson Pressure in the Average-Atom Model [28]. P_{contin}^{nr} is clearly positive. $f(x)$ is the Fermi-Dirac distribution function, i.e., $f(x) = 1/[1 + e^{(x-\mu)/k_B T}]$. For bound electrons, we find that

$$P_{\text{bound}} = \frac{\hbar^2}{24\pi m_e} \sum_{n\ell} 2(2\ell+1) f(\varepsilon_{n\ell}) \left\{ \left[\frac{d}{dr} \left(\frac{P_{n\ell}(r)}{r} \right) \right]^2 + \frac{2m_e}{\hbar^2} \varepsilon_{n\ell} \left(\frac{P_{n\ell}(r)}{r} \right)^2 + \frac{\ell(\ell+1)}{r^2} \left(\frac{P_{n\ell}(r)}{r} \right)^2 \right\}_{R_{WS}}. \tag{10}$$

Because $\varepsilon_{n\ell}$ takes negative values, P_{bound}^{nr} has no definite sign. For the ions, we use the ideal gas pressure.

To obtain the electronic electrical conductivity, we use the Kubo-Greenwood approach developed for the average-atom model [14–16]. Only the free-free component is considered. We have

$$\sigma(\omega) = \frac{2\pi e^2}{3\Omega\omega^3 m_e^2} \int_0^{+\infty} d\varepsilon [f(\varepsilon) - f(\varepsilon + \hbar\omega)] \sum_{\ell'=\ell\pm1} \ell_> \left[\int_0^{R_{WS}} dr P_{\varepsilon\ell}(r) \frac{dV_{ei}(r)}{dr} P_{\varepsilon+\hbar\omega\ell'}(r) \right]^2. \tag{11}$$

In this expression, $\Omega = 4\pi R_{WS}^3/3$ and $\ell_>$ is the maximum of ℓ and ℓ'

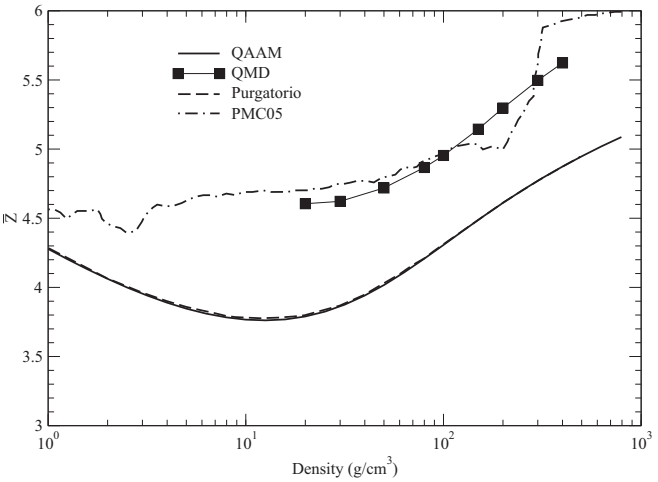

FIG. 1. Average ionization $\bar{Z}$ as a function of mass density in a carbon plasma at $T = 100$ eV. The QAAM values are compared to the QMD and PURGATORIO results. We have included the calculations of Potekhin *al.* [36] (PMC05) done at $T = 1\,000\,000$ K.

. We use the acceleration form to compute the matrix element [29]. This expression diverges as $1/\omega^2$ at small angular frequency ω. To avoid this problem, we multiply $\sigma(\omega)$ by $\omega^2/(\gamma^2+\omega^2)$. The free parameter γ is determined such that the sum rule [11]

$$\int_0^{+\infty} d\omega\sigma(\omega) = \frac{\pi e^2}{2m_e}\bar{Z}N_i \tag{12}$$

is respected [14]. By definition [2], the average ionization $\bar{Z} = \Omega\, n(R_{WS})$. A relativistic version of the QAAM code exists [27]. We do not use it because the relativistic effects are small in the present cases studied in this work. Note that we have a relativistic equation of state based on the QAAM code but not the relativistic extension of the free-free component of the electronic electrical conductivity.

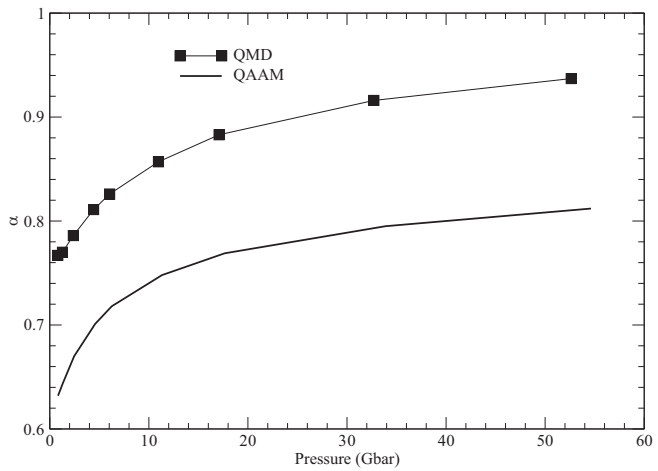

FIG. 2. $\alpha = \bar{Z}/Z$ as a function of pressure in a carbon plasma at $T = 100$ eV. The QAAM values are compared to the QMD results.

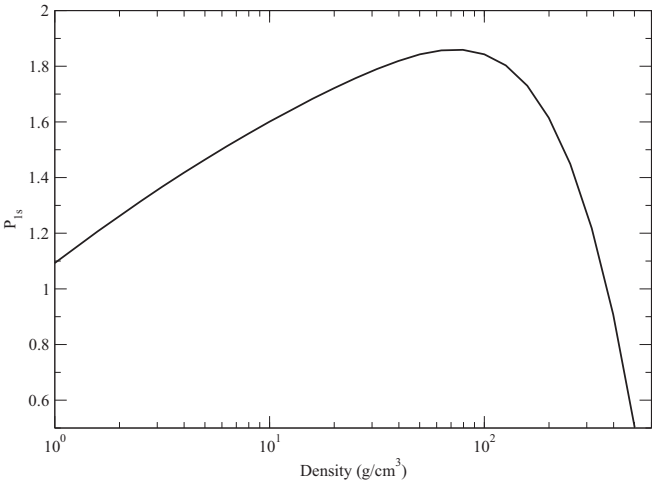

FIG. 3. Population of subshell 1*s* as a function of mass density in a carbon plasma at $T = 100$ eV obtained with QAAM.

B. Quantum molecular dynamics simulations

To compare data obtained with QAAM to results from QMD simulations, which treat the electrons within DFT, while describing the ions with classical molecular dynamics. In particular, we calculate the pressure from recently published carbon QMD data [8], which were computed using the Vienna Ab initio Simulation Package (VASP) [30–32]. The data set considered mass densities between 20 and 400 g/cm^3 at a temperature of $T = 100$ eV, which is extended for four additional mass densities (50 g/cm^3, 80 g/cm^3, 100 g/cm^3, and 150 g/cm^3) at $T = 150$ eV in this work. For the additional data points, we used the same simulation parameters as described by Bethkenhagen *et al.* [8], i.e., 32 carbon atoms thermostated with the Nosé-Hoover approach [33]. The electrons were described with the Perdew, Burke, and Ernzerhof [34] exchange-correlation functional and a Coulomb potential with a 15 keV energy cutoff was used. Each calculation at $T = 150$ eV was run for at least 20 000 time steps after equilibration with a time step size of 30 as and the k-point

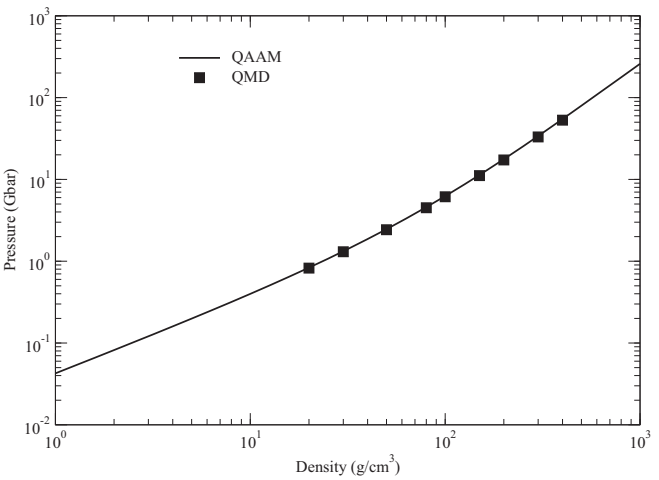

FIG. 4. Pressure as a function of mass density in a carbon plasma at $T = 100$ eV obtained with QAAM and QMD simulations.

TABLE I. Pressure P in Gbar, $\bar{Z}$, $\alpha = \bar{Z}/Z$, ε_{1s}, and μ as a function of the mass density ρ in g/cm^3 obtained with the QMD simulations and QAAM at $T = 100$ eV. ε_{1s} and μ are in Rydberg and are given only for QAAM (see text). (x) means 10^x.

ρ	P		$\bar{Z}$		α		ε_{1s}	μ
	QMD	QAAM	QMD	QAAM	QMD	QAAM	QAAM	QAAM
20	0.824	0.834	4.605	3.790	0.768	0.632	−15.3043	−1.8959
30	1.305	1.323	4.622	3.862	0.770	0.644	−13.5995	2.0286
50	2.427	2.463	4.719	4.017	0.787	0.670	−11.2755	7.7790
80	4.501	4.577	4.867	4.208	0.811	0.701	−8.9363	1.4281(1)
100	6.140	6.250	4.954	4.307	0.826	0.718	−7.7624	1.7942(1)
150	11.12	11.33	5.144	4.488	0.857	0.748	−5.5647	2.5880(1)
200	17.29	17.66	5.297	4.611	0.883	0.769	−4.0113	3.2801(1)
300	33.04	33.89	5.497	4.771	0.916	0.795	−1.9915	4.4966(1)
400	53.02	54.63	5.623	4.874	0.937	0.812	−0.8408	5.5779(1)

sample was performed with the Baldereschi mean-value point [35]. The pressure for each simulation was finally calculated as average over the entire trajectory containing an ideal gas contribution and an interaction term, which is calculated as trace of the stress-tensor obtained from the DFT part. In the latter, we applied an energy cutoff for the Coulomb potential of 100 keV instead of 15 keV to ensure the highest level of accuracy possible. To be more specific, the QAAM and the electronic part of QMD are indeed based on the same Kohn-Sham idea. However, QMD does not use spherical harmonics to construct the orbitals. It uses instead plane waves, which should be well suited for high-density systems. Note also that the carbon QMD simulations presented here are spin-degenerate, i.e., we do not treat spin explicitly at high temperature. This is the same thing for QAAM but at any temperature. QMD does not differentiate between bound and free electrons by construction. We only do that as soon as we start to calculate the ionization via the conductivity, where we have to make a choice what electrons to consider as free. In the actual QMD runs, we never differentiate between bound and free and also have all the bound-free transitions included explicitly within the adiabatic approximation. In QAAM, we consider explicitly bound and free electrons, but they are treated self-consistently in a quantum mechanical approach. The electronic pressure is made of two parts, a bound contribution and a free contribution. In QMD simulations, no such thing is done.

III. NUMERICAL APPLICATIONS

As a first application, we compare the average ionization $\bar{Z}$ found with the QAAM model to the ones obtained with the QMD simulations and the PURGATORIO code for a carbon plasma at $T = 100$ eV [8]. $\bar{Z}$ is plotted as a function of mass density in Fig. 1. We can see the excellent agreement between QAAM and PURGATORIO. QAAM is here nonrelativistic and PURGATORIO is relativistic. The small disagreement near the minimum may be due to this fact, but it is not certain since relativistic effects here are rather small. We confirm that QMD results are systematically about 0.5 higher than the average ionization predicted by the average-atom models. We have also plotted the Potekhin *et al.* [36] (PMC05) calculations at $T = 10^6$ K, so quite close to $T = 100$ eV. The curve is quite irregular, but it is in better agreement at high mass density with the QMD simulations than the predictions of the two average-atom models. The approach of Potekhin *et al.* [36] is based on the minimization of the free energy in the framework of the chemical picture, so quite different from the average-atom model. It is puzzling why there is such a discrepancy between the two groups of approaches, i.e., the QMD simulations and the PMC05 calculations and the QAAM and PURGATORIO results. We have no explanation to furnish right now to explain this fact. Maybe it is a many-body effect due to electronic correlations that is causing the deviation of 0.5 between the QMD simulations and the average-atom model results. In Fig. 2 we plot the values of $\alpha = \bar{Z}/Z$ as a function of pressure in a carbon plasma at $T = 100$ eV obtained by the QMD simulations and QAAM. Not surprisingly, we confirm the discrepancy between the QMD and the QAAM results for the average ionization. It is not clear why the QMD results are 0.5 higher than average ionization predicted by the average-atom models. The subshell $1s$ is significantly open in the QMD simulations compared to the average-atom model. To check this, we plot in Fig. 3 the population of subshell $1s$ as a function of mass density in a carbon plasma at $T = 100$ eV. We can see that near 100 g/cm^3, P_{1s} is close to 1.8, so we expect

TABLE II. Pressure P in Gbar as a function of the mass density ρ in g/cm^3 obtained with the QMD simulations and QAAM at $T = 150$ eV.

ρ	P	
	QMD	QAAM
50	3.513	3.546
80	6.141	6.193
100	8.129	8.190
150	13.89	14.00

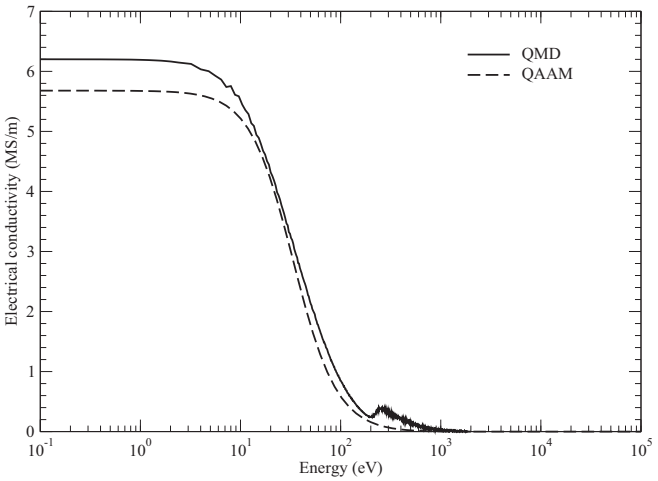

FIG. 5. Electrical conductivity as a function of energy in a carbon plasma at 50 g/cm^3 and $T = 100$ eV obtained with QAAM and QMD simulations using the Kubo-Greenwood approach.

an average ionization around 4.2 as is the case for QAAM and PURGATORIO in Fig. 1. We can see how subshell $1s$ is pressure ionized. The behavior of P_{1s} is consistent with the trend of $\bar{Z}$ in Fig. 1. Occupation numbers of subshells $2s$ and $2p$ are small and do not contribute much to $\bar{Z}$. Subshell $2p$ disappears between 2.5 and 3.2 g/cm^3, whereas subshell $2s$ does between 5 and 6.3 g/cm^3. Subshell $1s$ disappears between 501 and 631 g/cm^3. In Fig. 4 we compare the pressure obtained from QAAM and the QMD simulations. We can see the good agreement between the two approaches. Note that we are using the same methods to calculate the electronic and ionic components of the pressure, so the comparison between the QMD simulations and QAAM really makes sense. QAAM performs very well compared to QMD simulations. The only difference concerns the electronic part. In the QAAM approach, we are using a 1D spherically symmetric description of the electronic density, whereas in the QMD simulations,

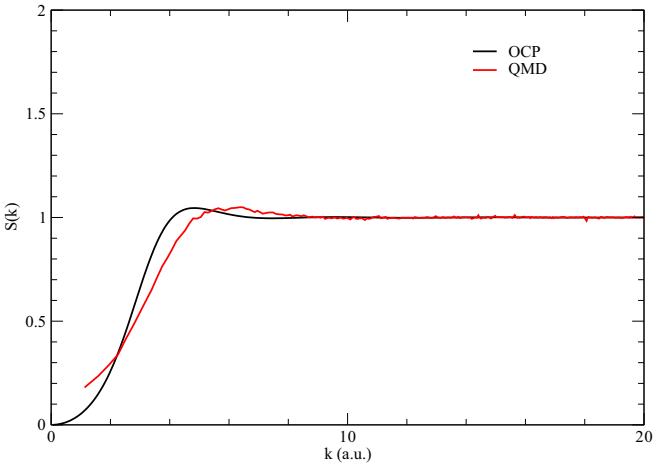

FIG. 6. Structure factor $S(k)$ as a function of the wave number k in a carbon plasma at 50 g/cm^3 and $T = 100$ eV obtained using an OCP model or extracted from the QMD simulations. k is in atomic units (a.u.).

we consider a 3D description of the electronic density. In the present work, 3D effects could be important since the carbon plasma in our thermodynamic conditions may be not so simple. What is tricky with the average ionization predicted by the QMD simulations is that it is based on the electrical conductivity, which is not strictly related to the pressure. So we may have a higher effective average ionization coming from the QMD simulations compared to the QAAM code and at the same time have close predictions concerning the QMD and QAAM pressures. It would be better to speak of effective average ionization. It would be great to have the pressure as predicted by the PURGATORIO code using either the differentiation of the free energy or the virial theorem [37] or using the stress-tensor method. Unfortunately, we do not have it [8]. We can fit the pressure values obtained with QAAM as a function of mass density with the formula $\log_{10}[P(\text{Mbar})] = h\{\log_{10}[\rho(\text{g/cm}^3)]\}$ where ρ is the mass density and

$$h(x) = 1.63013 + 0.921541x + 0.0894653x^2 - 0.100441x^3 + 0.071916x^4 - 0.0119356x^5. \quad (13)$$

$\log_{10}(x)$ is the logarithm with base 10 of x. In Table I we give the values of pressure, average ionization, and α as a function of mass density for the QMD simulations and QAAM. We give also ε_{1s} and μ for the QAAM code. We do not present ε_{1s} and μ for QMD simulations since a ε_{1s} for an effective single ionic particle is difficult to extract for a system of many ionic particles in the simulation box and μ may not have a real meaning that could be compared to corresponding QAAM values. In Table II we give the pressure obtained with the QMD simulations and QAAM for various mass densities at $T = 150$ eV. The agreement between the two approaches is very good. The QMD and QAAM pressures are more or less the same because we are using the same method to calculate the electronic pressure, i.e., the stress-tensor approach. To our knowledge, this is the first comparison of QMD simulations and the average-atom model using the same technique to calculate the electronic pressure and the same treatment for the ions. Note that the QMD method is not so *ab initio* because the ions in VASP are described using the ideal gas law. This may be questionable at low temperature. We also give in Table III $\bar{Z}$ derived from the Friedel Sum Rule (FSR) [27] as well as the FSR corresponding to Table I. We can see that $\bar{Z}$ is decreasing function with increasing density. We can see that the FSR is well satisfied since we obtain results close to 6. The contribution of bound and free electronic densities beyond the Wigner-Seitz radius is small, and the phase shifts are well calculated as can be seen below for a specific example. At 50 g/cm^3 and $T = 100$ eV, $\bar{Z} = 4.67$ for the QMD simulations whereas $\bar{Z} = 4.02$ with QAAM. At this thermodynamic condition, we plot in Fig. 5 the dynamic electronic electrical conductivity as a function of energy calculated with the Kubo-Greenwood approach using QMD simulations and QAAM. We can see some disagreement between the two approaches if we keep in mind that the average ionization predicted by the QMD simulations is higher than the one given by QAAM and that this approach considers only the free-free component. This explains why the QMD curve at low energy is higher that the QAAM curve. In this regime, the QAAM

TABLE III. $\bar{Z}$ from the Friedel sum rule (FSR) and the FSR as a function of the mass density ρ in g/cm^3 obtained with QAAM at $T = 100$ eV.

ρ	$\bar{Z}$	FSR
20	4.289	6.012
30	4.228	6.014
50	4.158	6.018
80	4.104	6.023
100	4.084	6.025
150	4.057	6.030
200	4.046	6.032
300	4.037	6.034
400	4.034	6.033

conductivity is nearly Drude-like. With this approach, we obtain $\sigma(0) = 5.68$ MS/m. The Ziman-Evans [3–5] formula gives $\sigma(0) = 5.65$ MS/m. We have used a one-component plasma structure factor derived from $\bar{Z}$ in this approach. For the structure factor, we have used the fit provided by Bretonnet and Derouiche [38]. In these thermodynamic conditions, the plasma coupling parameter is equal to 5.09. The ionic system is thus moderately coupled. We plot in Fig. 6 the structure factor calculated using the Bretonnet and Derouiche [38] formula and its value extracted from the QMD simulations. We can see that the agreement is quite good. In our calculations using the Ziman-Evans formula, we did not remove the "crystalline component" from the OCP structure factor, as proposed by Wetta and Pain [39], because we do not know how to do this without using an approximate expression such as the hypernetted-chain equations for charged spheres in the liquid state. In the QMD simulations, the structure factor is calculated down to 2 Å^{-1}. We plot in Fig. 7 the phase shifts as a function of the wave number k up to $\ell = 15$. The wave number k is in atomic units (a.u.). We can see that only a limited number of phase shifts really matter. We have shown the s, p, and d phase shifts. All the phase shifts as a function of k are smooth. As for QMD simulations, we obtain a $\sigma(0) = 6.20$ MS/m using a Drude fit for small energies. Note that we cannot use QAAM to estimate an average ionization from the sum rule as was done in QMD simulations due to the divergence of the electronic electrical conductivity at low energy. By construction, the method proposed in Ref. [8] gives the average-atom ionization $\bar{Z}$. We plot in Fig. 8 the static electrical conductivity as a function of density in a carbon plasma at $T = 100$ eV obtained with QAAM code and QMD simulations using the Kubo-Greenwood approach (KG) or the Ziman-Evans (ZE) method. We can see the QMD results are always higher than the QAAM results as expected. Moreover, in this example, QAAM results using either ZE or KG approaches are quite close to each other, especially at low density. We do not recover the results published recently by Dharma-wardana using either the Thomas-Fermi Lee and More method or the Neutral Pseudo-Atom (NPA) model using the Ziman approach [40]. More specifically, our electrical conductivity increases with density and does not show any maximum as can be found in the paper by Dharma-wardana [40] for the NPA Ziman case. The difference between QMD KG and QAAM KG is due to the average ionization. It would be great to have comparisons of electrical conductivity with the PURGATORIO code. In this work, we go beyond the seminal results of Ref. [8] since we can compare results between

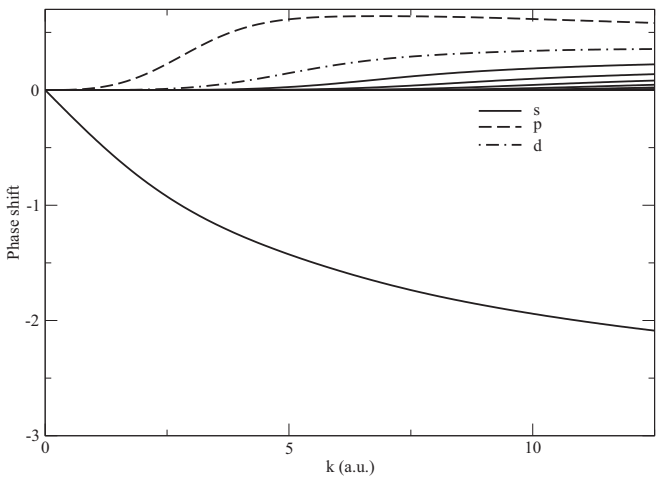

FIG. 7. Phase shifts as a function of the wave number k in a carbon plasma at 50 g/cm^3 and $T = 100$ eV obtained with the QAAM model. k is in atomic units (a.u.).

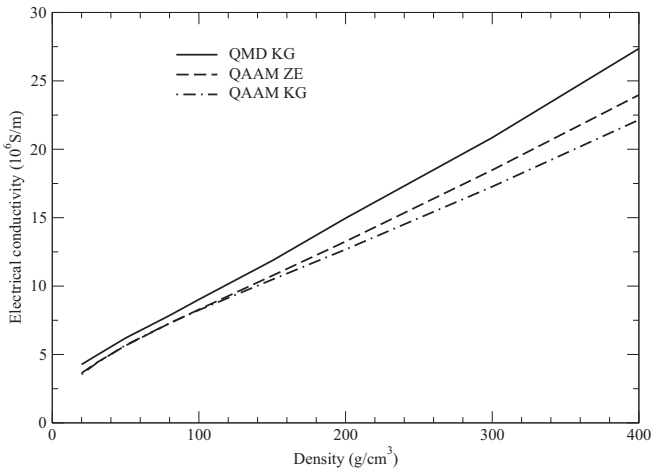

FIG. 8. Static electrical conductivity as a function of density in a carbon plasma at $T = 100$ eV obtained with QAAM and QMD simulations using the Kubo-Greenwood approach (KG) or the Ziman-Evans (ZE) method.

the QMD simulations and the QAAM code for two quantities, the pressure and the electrical conductivity. Moreover, we consider two types of calculation of the electrical conductivity with the QAAM code, the Ziman-Evans approach and the Kubo-Greenwood method. They are plainly consistent with each other.

IV. CONCLUSION

We have compared calculations of average ionization, pressure, and electronic electrical conductivity obtained with a nonrelativistic average-atom model with QMD simulations for a carbon plasma. We confirm the disagreement between the QMD results for the average ionization with the average-atom model. This is not easy to understand why it is such so. This disagreement is also seen concerning the electronic electrical conductivity, both of which are obtained with the Kubo-Greenwood approach. Maybe the concept of splitting bound and free components as done in QMD does not fully account for *e-e* collisions or maybe there is a missing many-body or 3D effects in the average-atom model. Our results for the average ionization are in excellent agreement with the PURGATORIO code. As for pressure, a better agreement is obtained between our average-atom model and the QMD simulations in the gigabar regime.

ACKNOWLEDGMENTS

The QMD calculations were performed at the North-German Supercomputing Alliance (HLRN) facilities.

[1] M. S. Murillo, J. Weisheit, S. B. Hansen, and M. W. C. Dharma-wardana, Phys. Rev. E **87**, 063113 (2013).
[2] R. M. More, Adv. At. Mol. Phys. **21**, 305 (1985).
[3] G. A. Rinker, Phys. Rev. B **31**, 4207 (1985); **31**, 4220 (1985).
[4] F. Perrot and M. W. C. Dharma-wardana, Phys. Rev. A **36**, 238 (1987).
[5] G. A. Rinker, Phys. Rev. A **37**, 1284 (1988).
[6] G. Faussurier and C. Blancard, Phys. Rev. E **91**, 013105 (2015).
[7] J. Clérouin, P. Noiret, P. Blottiau, V. Recoules, B. Siberchicot, P. Renaudin, C. Blancard, G. Faussurier, B. Holst, and C. E. Starrett, Phys. Plasmas **19**, 082702 (2012).
[8] M. Bethkenhagen, B. B. L. Witte, M. Schörner, G. Röpke, T. Döppner, D. Kraus, S. H. Glenzer, P. A. Sterne, and R. Redmer, Phys. Rev. Res. **2**, 023260 (2020).
[9] R. Kubo, J. Phys. Soc. Jpn. **12**, 570 (1957).
[10] D. A. Greenwood, Proc. Phys. Soc. **71**, 585 (1958).
[11] M. P. Desjarlais, J. D. Kress, and L. A. Collins, Phys. Rev. E **66**, 025401(R) (2002).
[12] B. Wilson, V. Sonnad, P. Sterne, and W. Isaacs, J. Quant. Spectrosc. Radiat. Transfer **99**, 658 (2006).
[13] P. A. Sterne, S. B. Hansen, B. G. Wilson, and W. A. Isaacs, High Energy Density Phys. **3**, 278 (2007).
[14] W. R. Johnson, C. Guet, and G. F. Bertsch, J. Quant. Spectrosc. Radiat. Transfer **99**, 327 (2006).
[15] C. E. Starrett, High Energy Density Phys. **19**, 58 (2016).
[16] A. A. Ovechkin, P. A. Loboda, and A. L. Falkov, High Energy Density Phys. **20**, 38 (2016).
[17] G. Faussurier and C. Blancard, Phys. Rev. E **99**, 053201 (2019).
[18] T. Blenski and K. Ishikawa, Phys. Rev. E **51**, 4869 (1995).
[19] W. R. Johnson, J. Nilsen, and K. T. Cheng, Phys. Rev. E **86**, 036410 (2012).
[20] P. Hohenberg and W. Kohn, Phys. Rev. **136**, B864 (1964).
[21] W. Kohn and L. J. Sham, Phys. Rev. **140**, A1133 (1965).
[22] N. D. Mermin, Phys. Rev. **137**, A1441 (1965).
[23] S. Ichimaru, H. Iyetomi, and S. Tanaka, Phys. Rep. **149**, 91 (1987).
[24] U. Gupta and A. K. Rajagopal, Phys. Rev. A **21**, 2064 (1980).
[25] F. Salvat, J. M. Fernández-Varea, and W. Williamson. Jr., Comput. Phys. Commun. **90**, 151 (1995).
[26] W. Eissner, Comput. Phys. Commun. **114**, 295 (1998).
[27] G. Faussurier and C. Blancard, Phys. Plasmas **28**, 042710 (2021).
[28] W. Johnson, University of Notre Dame, South Bend, IN, homepage, http://www3.nd.edu/~johnson/.
[29] I. I. Sobelman, *Atomic Spectra and Radiative Transitions*, 2nd ed. (Springer-Verlag, Berlin, 1992).
[30] G. Kresse and J. Hafner, Phys. Rev. B **47**, 558(R) (1993).
[31] G. Kresse and J. Hafner, Phys. Rev. B **49**, 14251 (1994).
[32] G. Kresse and J. Furthmüller, Phys. Rev. B **54**, 11169 (1996).
[33] S. Nosé, J. Chem. Phys. **81**, 511 (1984).
[34] J. P. Perdew and K. Burke, and M. Ernzerhof, Phys. Rev. Lett. **77**, 3865 (1996).
[35] A. Baldereschi, Phys. Rev. B **7**, 5212 (1973).
[36] A. Y. Potekhin, G. Massacrier, and G. Chabrier, Phys. Rev. E **72**, 046402 (2005).
[37] D. A. Liberman, Phys. Rev. B **20**, 4981 (1979).
[38] J.-L. Bretonnet and A. Derouiche, Phys. Rev. B **38**, 9255 (1988).
[39] N. Wetta and J.-C. Pain, Phys. Rev. E **102**, 053209 (2020).
[40] M. W. C. Dharma-wardana, Phys. Rev. E **104**, 015201 (2021).